Available online at www.sciencedirect.com
ScienceDirect
Optical Materials 30 (2008) 1840–1847
OPTICAL Materials
www.elsevier.com/locate/optmat

Photoluminescent emission of Pr^{3+} ions in different zirconia crystalline forms

F. Ramos-Brito [a,*], C. Alejo-Armenta [a], M. García-Hipólito [b], E. Camarillo [c], J. Hernández A [c], H. Murrieta S [c], C. Falcony [d]

[a] *Laboratorio de Materiales Optoelectrónicos, DIDe, Centro de Ciencias de Sinaloa, Av. de Las Américas No. 2771 Nte. Col. Villa Universidad. 80010 Culiacán, Sinaloa, Mexico*
[b] *Instituto de Investigaciones en Materiales, Universidad Nacional Autónoma de México, A.P. 70-360 Coyoacán 04510 DF, Mexico*
[c] *Instituto de Física, Universidad Nacional Autónoma de México, A.P. 20-364 Del. A. Obregón 01000 DF, Mexico*
[d] *Departamento de Física, CINVESTAV-IPN, A.P. 14-740 G.A. Madero 07000 DF, Mexico*

Received 9 August 2007; received in revised form 28 November 2007; accepted 5 December 2007
Available online 30 January 2008

Abstract

Polycrystalline praseodymium doped-zirconia powders were synthesized by crystallization of a saturated solution and annealed in air at $T_a = 950$ °C. Monoclinic, tetragonal and cubic crystalline phases of zirconia were obtained. EDS studies showed homogeneous chemical composition over all the powders particles and chemical elemental contents in good agreement with the incorporation of Pr^{3+} ion in Zr^{4+} sites. XRD patterns showed stabilization of tetragonal and cubic phases at 1.28 and 2.87 at.% of Pr^{3+} doping concentrations, respectively. Both unit cells expand when Pr^{3+} content increases. All samples showed a crystallite size lower than 27 nm. Diffuse reflectance studies exhibited the presence of the 4f5d absorption band of Pr^{3+}, and absorption peaks in 440–610 nm region associated with 4f inter-level electronic transitions in Pr^{3+} ion. Low temperature (20 K) photo-luminescent spectroscopic measurements over excitation of 488 nm for praseodymium doped zirconia, showed multiple emission peaks in the 520–900 nm range of the electromagnetic spectrum, associated with typical 4f inter-level electronic transition in Pr^{3+}. Incorporation of Pr^{3+} in more than one zirconia crystalline phase and the incorporation in cubic C_2 sites, were observed. Zirconia powders presented significant differences in its emission spectra as a function of the type of crystalline phase compounds.

PACS: 32.30.–r; 32.30.Jc; 32.50.+d; 71.30.+h; 71.70.–d; 78.45.+h; 78.55.–m

Keywords: Praseodymium; Photoluminescence; 4f5d Absorption; Cubic zirconia; Tetragonal zirconia

1. Introduction

Metallic oxides (MO) present good chemical stability and wide energy gap which is commonly affected with the incorporation of activator ions, generally to provide new optical properties or to enhance its intrinsic ones [1–4]. Rare earth (RE) ions have been considered the most important optical activators for luminescent devices [5]. The consequent appearance of deep electronic states, due to the incorporation of RE in MO crystalline structure, provides to this rare earth doped metallic oxide (MO:RE) luminescent properties and consequent emissions in the visible range of electromagnetic spectrum, preserving and some times enhancing the intrinsic properties of the MO. This is probably why, in the last decade, trivalent rare earth doped metallic oxides ($MO:RE^{3+}$) have gained popularity like the most promissory luminescent materials [5]. The fluorescent emission in $MO:RE^{3+}$ commonly comes from 5d–4f or 4f–4f electronic transitions in rare earth ions. Commonly, the responsible of the emission are the rare

* Corresponding author. Tel.: +52 667 7599000x1178/1177; fax: +52 667 7599011.
E-mail address: rbrito@correo.ccs.net.mx (F. Ramos-Brito).

0925-3467/$ - see front matter © 2007 Elsevier B.V. All rights reserved.
doi:10.1016/j.optmat.2007.12.001

earth ions. Among advanced ceramic materials, zirconia (ZrO_2) plays an important role due to its superior hardness, high refractive index, optical transparency, chemical stability, photothermal stability, high thermal expansion coefficient, low thermal conductivity, ionic conductivity, polymorphic nature, and high thermomechanical resistance; it can be used in a variety of photonics and industrial applications [6]. Furthermore the low phonon energy of ZrO_2 decreases the probability of non-radiative multiphonon relaxation of excited rare-earth activator ions throughout the vibrational bands of the host lattice, which is considered one of the most competitive non-radiative relaxation processes for optical activator ions in a luminescent material. Many studies on zirconia stabilization [7,8] have been done considering the effects of impurities, since activator content determines whether the tetragonal or the cubic phase will be stabilized. Trivalent rare earth ions have been used, besides a structure stabilization action [9,10], as luminescence activators in single crystal zirconia [11–16] and polycrystalline zirconia films [17–19]. Extensive studies have been performed for the preparation of stabilized zirconia ceramics using different routes because the synthesis method is crucial to optimise the properties of zirconia ceramics [20].

The present work reports on the influence of the doping concentration on the crystalline structure and photoluminescent properties of praseodymium doped zirconia powders obtained by crystallization of a saturated solution.

2. Experimental

Polycrystalline powders of praseodymium doped zirconia were prepared by crystallization of a saturated solution followed by a post annealing treatment at 950 °C [21]. The precursor solution was composed by zirconium nitrate ($ZrO(NO_3)_2 \cdot xH_2O$ Aldrich Co.) and ethyl alcohol. Doping with Pr^{3+} was achieved by adding $Pr(NO_3)_3 \cdot 6H_2O$ to the precursor solution in the range from 1 to 20 at.% in relation to the zirconium nitrate content in this solution. Particle size and qualitative shape measurements were performed by scanning electron microscopy (SEM), and chemical composition characterization using energy dispersive spectroscopy (EDS), both with a Leica Cambridge Stereoscan 440 electron microscope equipped with a beryllium window X-ray detector. The crystalline structure was analyzed by X-ray diffraction (XRD), using a Siemens D-5000 with Cu K_α radiation (1.5426 Å). Identification of tetragonal and cubic phases, and indexing of the peaks in the XRD patterns was done employing the equations: $\sin^2\theta = A(h^2 + k^2) + Cl^2$ for tetragonal and $\sin^2\theta = A(h^2 + k^2 + l^2)$ for cubic phase, where A ($= \lambda^2/4a^2$) and C ($= \lambda^2/4c^2$) are constants for any peak in the corresponding diffractogram [22]. Crystallite size of the powders was obtained using Scherrer's formula: $t = (0.9\ \lambda)/(B\cos\theta_B)$ for peaks which 2θ were $< 35°$. Diffuse photoreflectance studies in the UV–VIS-NIR were carried out using a spectrophotometer Cary 5000-Varian. Low temperature (20 K) photoluminescence emission spectra were recorded using a conventional setup. The 488 nm argon laser line was used like excitation source. The sample was placed in a mobile holder for aligning purposes and the emission was collected perpendicular to the pumping signal. A 0.5 m monochromator (Acton Research) was used to scan the emission spectrum which was measured using a photomultiplier tube connected to a PC via a lock-in amplifier.

3. Results and discussion

3.1. Chemical composition and crystalline analysis

Polycrystalline powders of praseodymium doped zirconia were obtained by the crystallization of a saturated solution process, varying the Pr^{3+} doping concentration parameter. The Table 1 shows the chemical composition of the powders as a function of $Pr(NO_3)_3 \cdot 6H_2O/ZrO(NO_3)_2 \cdot xH_2O$ ratio in the precursor solution. A chemical analysis of different zones of the powder, which were selected in a random way, shows a homogeneous chemical composition over all the powder particles. The chemical element contents at whatever concentrations of $Pr(NO_3)_3 \cdot 6H_2O$, is in good agreement with zirconium oxide rich in oxygen. The changes in elemental contents as the $Pr(NO_3)_3 \cdot 6H_2O$ percent increases, suggest the possible incorporation of Pr^{3+} ion in Zr^{4+} sites. Images obtained by SEM, but not showed for the sake of brevity, show: (1) a very broad particle size distribution in a range of 10 and 80 μm, being 40 μm the most common size, and (2) particles of flake shape with sharp edges and flat surface morphology. The morphology and the wide variety of particle sizes were associated with the grinding process. Fig. 1 shows XRD measurements and the evolution of the crystalline structure of zirconia as a function of $Pr(NO_3)_3 \cdot 6H_2O$ in precursor solution, here X in the PrX label indicates the percent of praseodymium nitrate hexa-hydrated in relation to the zirconium nitrate content in this solution. The XRD pattern for undoped zirconia powder, Pr 0 spectrum, shows

Table 1
Elemental chemical composition of praseodymium doped zirconia powders as a function of $Pr(NO_3)_3 \cdot 6H_2O/ZrO(NO_3)_2 \cdot xH_2O$ ratio in the precursor solution

$Pr(NO_3)_3 \cdot 6H_2O/ZrO(NO_3)_2 \cdot xH_2O$ ratio in the precursor solution	Oxygen (at.%)	Zirconium (at.%)	Praseodymium (at.%)
0.000	73.15	26.85	0
0.010	73.45	26.19	0.35
0.020	75.34	24.10	0.56
0.030	76.03	23.13	0.84
0.040	75.77	22.94	1.28
0.075	74.49	23.29	2.22
0.100	75.41	21.72	2.87
0.150	72.88	22.37	4.76
0.200	74.43	20.25	5.33

The measurements are in atomic percent (at.%). Results were obtained by EDS.

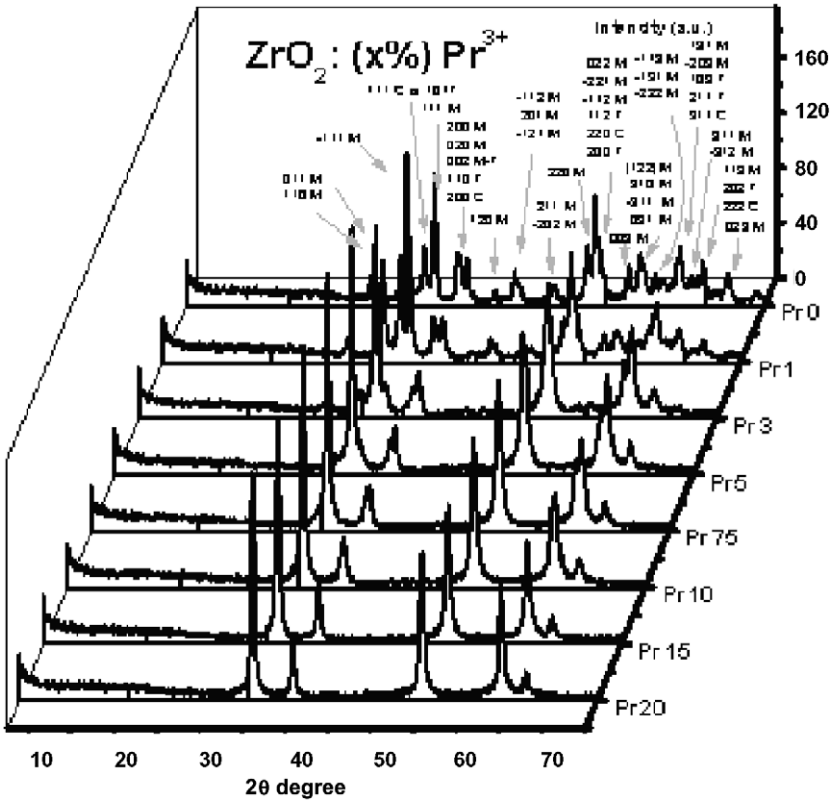

Fig. 1. XRD patterns of praseodymium doped zirconia powders as a function of Pr $(NO_3)_3 \cdot 6H_2O$ percent content in the precursor solution. X in Pr X spectra label means the Pr $(NO_3)_3 \cdot 6H_2O$ percent content. Figure shows Miller indexes for undoped zirconia powder Pr 0, with a crystalline structure composed by: Monoclinic (M), Tetragonal (T), and Cubic (C) phases.

multiple peaks associated with a polycrystalline structure composed by three crystalline phases: monoclinic, tetragonal and cubic, being monoclinic in major quantity. The relative close distance between peaks associated with tetragonal and cubic phases of zirconia does not allow discern, in this spectrum, between these two phases. The aggregation of praseodymium nitrate in the precursor solution, results in intensity decreases of the peaks associated with monoclinic phase, which vanish for 5 percent, being the tetragonal peaks the only ones present in the Pr 5 spectrum [23] (1.28 at.% of Pr^{3+} in zirconia powder, as measured by EDS). The crystalline structure for Pr 5 sample resulted in a tetragonal type I with lattice parameters of: $a = 3.60$ Å and $c = 5.17$ Å (see Fig. 2a). An evolution of crystalline structure from tetragonal I, Pr 5, to cubic F phase, Pr 10, was also observed, and was associated to praseodymium ion increasing concentration in zirconia powder, from 1.28 at.%, for tetragonal I phase, to 2.87 at.%, for cubic F phase (see Fig. 2b). Powders with contents of Pr^{3+} higher than 2.87 at.% remain cubic F crystalline phase. Fig. 3 shows a schematic representation of the XRD measurements corresponding to Pr 5, Pr 7.5, Pr 10, Pr 15 and Pr 20. A shift of the peaks in the diffraction pattern to lower 2θ values with the incorporation of Pr^{3+} ion, and without changes in the full-width at half maximum (FWHM) of the peaks was observed, which indicates a uniform expansion in the directions corresponding to the peaks involved, in the corresponding unit cell: tetragonal for Pr 5 and Pr 7.5; and cubic for Pr 10, Pr 15 and Pr 20. The last one resulted in a uniform expansion in all cubic directions. The Pr 10, Pr 15 and Pr 20 samples had lattice parameter "a" values of: 5.16, 5.18 and 5.20 Å for 2.87, 4.76 and 5.33 at.% concentration of Pr^{3+} ion in zirconia powder, respectively. The chemical composition results and the behavior on the crystal structure of doped zirconia as Pr^{3+} content increases, indicate the stabilization of the cubic phase of zirconia which was associated with the incorporation of Pr^{3+} ions in Zr^{4+} sites and the consequent creation of oxygen vacancies for charge compensation [24]. Little variation in the intensity of the peaks, in the XRD pattern, as Pr^{3+} content rises indicates unappreciable changes in the crystalline structure of the powders. Material growing in some preferred orientation (hkl) as a function of the Pr^{3+} ion concentration was not observed. Crystallite size values for different concentrations of Pr^{3+} ion were: Pr 0:26 nm; Pr 1:27 nm; Pr 3, Pr 5, Pr 7.5, Pr 10 and Pr 15:21 nm; and Pr 20:23 nm. Due to the homogeneity of the precursor mixture, the crystallization during the annealing treatment occurred probably by homogeneous nucleation mechanism delaying the growth of crystallites. The percent of tetragonal and/or cubic phase present in undoped zirconia sample, Pr 0, was associated to its crystallite size lower than Garvie critic size (30 nm) [25] where martensitic transformation $ZrO_{2\text{-tetragonal}} \rightarrow ZrO_{2\text{-monoclinic}}$ occurs. For praseodymium

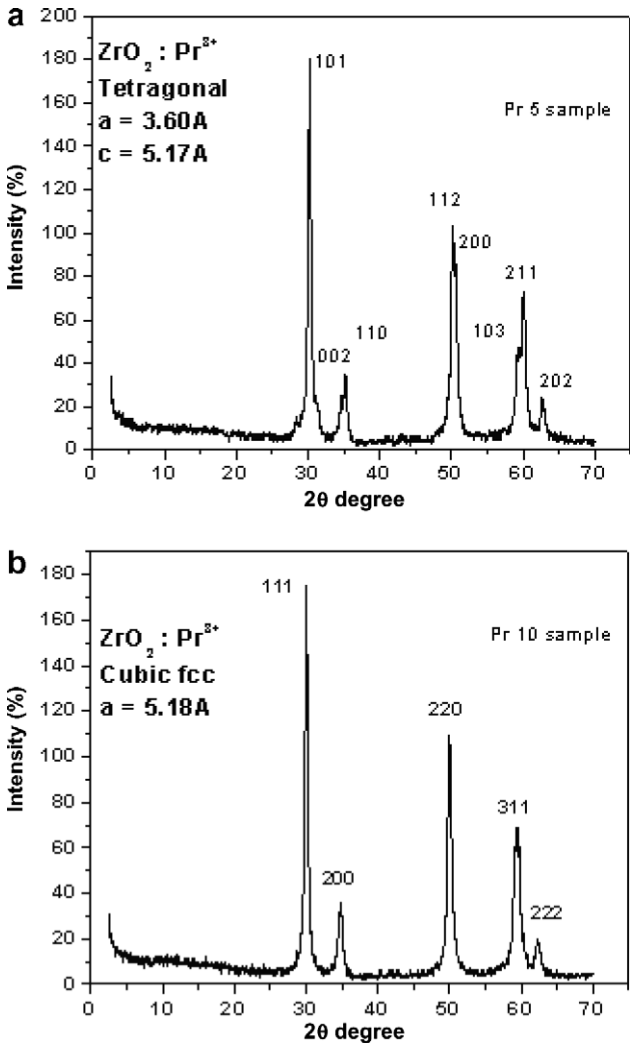

Fig. 2. Indexed XRD patterns for tetragonal I(a) and cubic F(b) zirconia powders, obtained from precursor solutions with 5 and 10 percent of Pr $(NO_3)_3 \cdot 6H_2O$ in relation to $ZrO(NO_3)_2 \cdot xH_2O$, respectively.

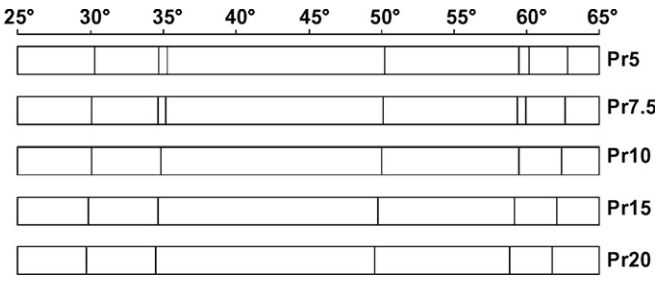

Fig. 3. Schematic representation of the XRD lines of praseodymium doped zirconia powders as a function of Pr $(NO_3)3 \cdot 6H_2O$ percent content in the precursor solution. X in Pr X spectra label means the Pr $(NO_3)_3 \cdot 6H_2O$ percent content in relation to $ZrO(NO_3)_2 \cdot xH_2O$ content. A notable sliding of the peaks to lower 2θ values can be observed.

doped zirconia samples the crystallite size and praseodymium stabilizer effects were complementary factors to increase the percent contents of cubic and/or tetragonal phases.

3.2. Diffuse reflectance and photoluminescent spectroscopy

Fig. 4 shows the diffuse reflectance spectra for praseodymium doped zirconia powders as a function of $Pr(NO_3)_3 \cdot 6H_2O$ in the precursor solution in relation to the zirconium nitrate content in this solution. All spectra were obtained using the spectrum for undoped zirconia powder like base line. A wide absorption band centered at 380 nm was observed in all spectra. For samples obtained from precursor solutions with praseodymium nitrate concentrations lower than 7.5% the 380 nm band has constant intensity, for upper concentrations than 7.5% the intensity starts to decrease and the apparition of a new band was observed. The position of this new band depends on praseodymium nitrate concentration and was centered at: 299, 295 and 292 nm for Pr 10, Pr 15 and Pr 20 samples (see zoom 1 of Fig. 4), respectively. This band was attributed to the $4f^3 \rightarrow 4f^25d$ absorption of Pr^{3+}ions. The 380 nm wide absorption band was associated with deep energy levels in zirconia energy gap due to the creation of crystal defects with the incorporation of Pr^{3+}. The existence of the 380 nm band and the overlapping of Pr^{3+} absorption peaks with part of this wide band, observed in the excitation spectrum for praseodymium doped zirconia composed by a mix of monoclinic, tetragonal and cubic crystalline phases, was reported before, proving the charge transfer between the host lattice and the activator ion [21].

The decreasing intensity of the 380 nm absorption band, with the increase of Pr^{3+} ions in zirconia, starting when zirconia adopt a well defined cubic phase (for Pr^{3+} ion concentrations upper than 2.87 at.%), was associated with two possible factors: (a) A lower number of defects on structure, which should have a consequent decrease on charge transfer effect, (b) A preferential absorption through the 4f5d band, which is associated with the increase on intensity of the ~290 nm absorption band. The lower emission intensity and the appearance of the intrinsic emission of zirconia for cubic zirconia samples (Fig. 5 – Pr 15), confirm the low efficiency of charge transfer process. In relation to spectroscopic studies of europium doped zirconia [24] and to the similar characteristics between Pr^{3+} and Eu^{3+} ions (ionic radius: Pr = 1.09, Eu = 1.12; electronegativity: Pr = 1.1, Eu = 1.0) exist a high possibility to have the majority of Pr^{3+} ions located in C_2 symmetry sites of cubic zirconia. The 299, 295 and 292 nm bands present in the absorption spectra of Pr 10, Pr 15 and Pr 20 cubic F samples were attributed to the $4f^3 \rightarrow 4f^25d$ absorption of Pr^{3+}ions located in C_2 sites [26], which on the other hands support the occupation of C_2 sites by the Pr^{3+} ions. Increase on intensity of $4f^3 \rightarrow 4f^25d$ absorption band when Pr^{3+} ion content rises, from 2.87 at.% to 5.33 at.%, suggest an increase on occupation of cubic C_2 sites by Pr^{3+} ions, and the possible preference of this site by incorporated Pr^{3+} ions. The high influence on the position of $4f^3 \rightarrow 4f^25d$ absorption band due to crystal field changes has been reported [26]. The shift in the position of this band, from

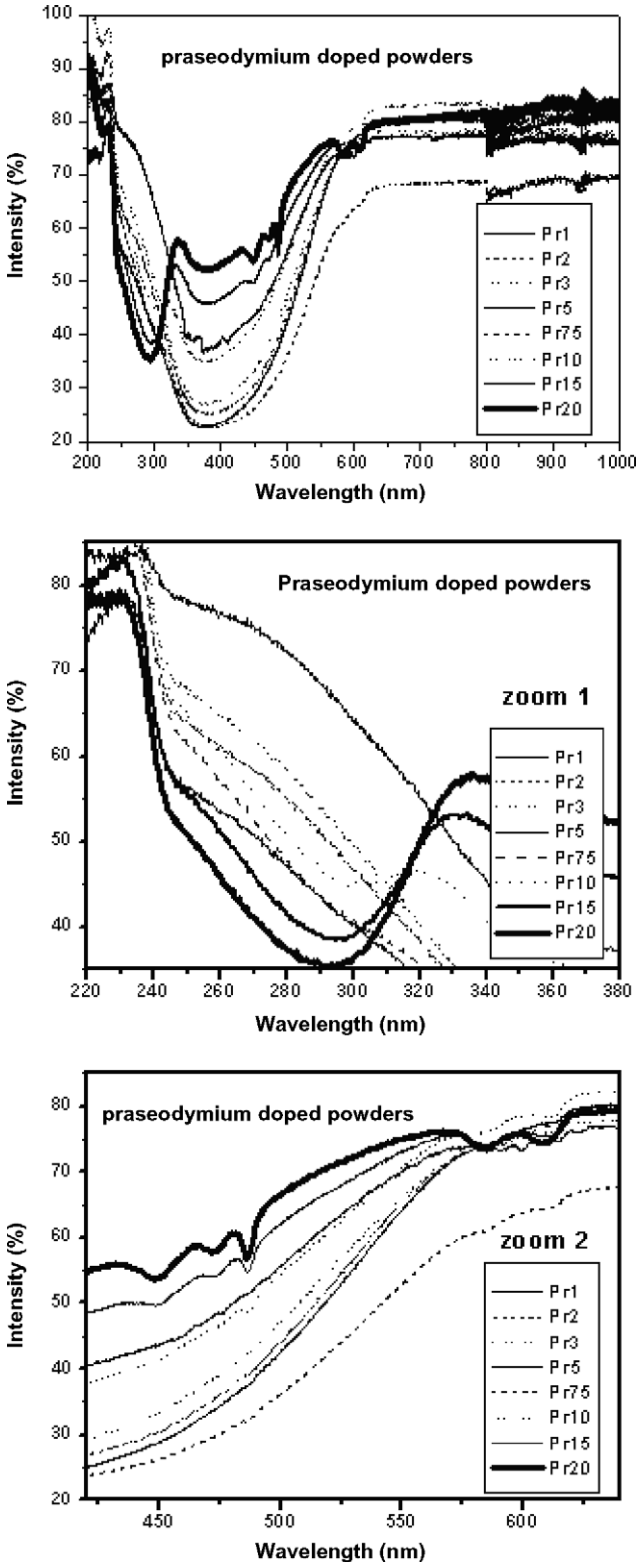

Fig. 4. Diffuse reflectance spectra of praseodymium doped zirconia powders as a function of Pr $(NO_3)_3 \cdot 6H_2O$ percent content in the precursor solution. X in Pr X spectra label means the Pr $(NO_3)_3 \cdot 6H_2O$ percent content in relation to $ZrO(NO_3)_2 \cdot xH_2O$ content. Zoom 1 and zoom 2 are amplifications of two different regions of the figure.

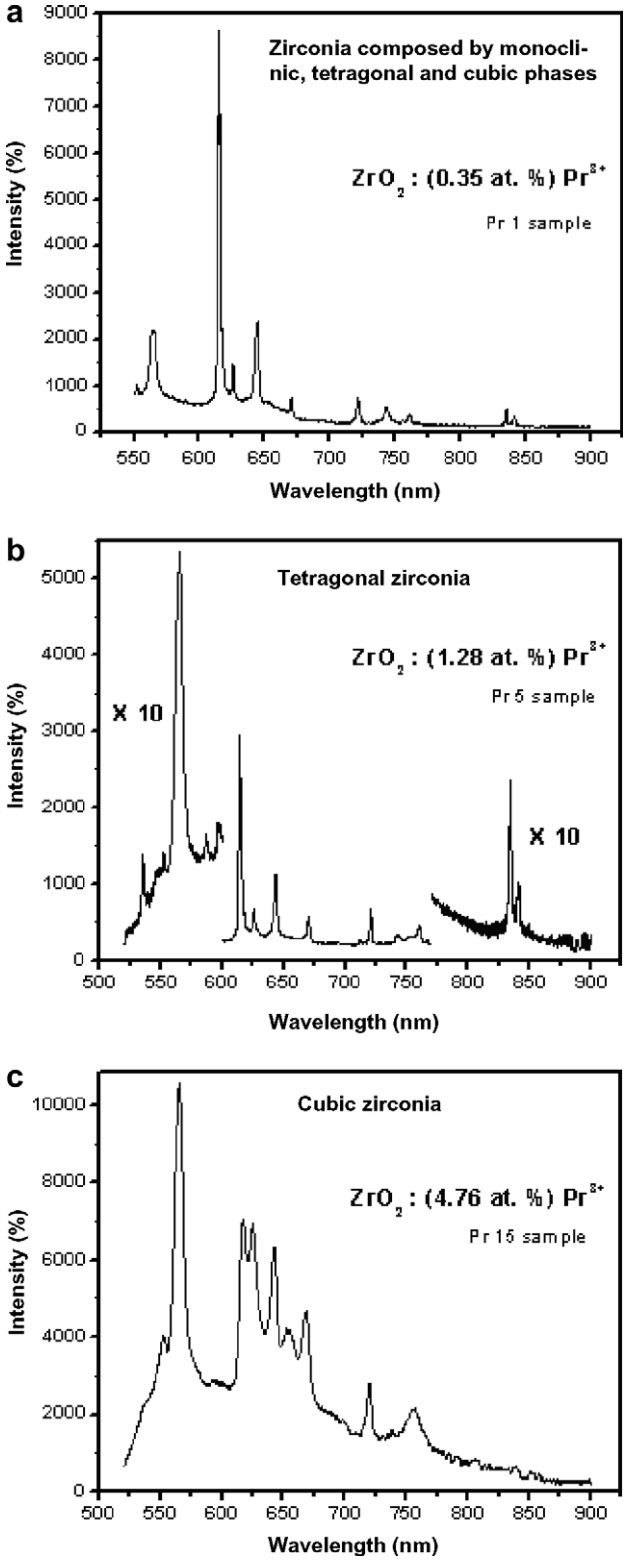

Fig. 5. Photoluminescent emission from three different zirconia powders whose phase compositions are: (a) monoclinic/tetragonal/cubic mixed phase, (b) tetragonal and (c) cubic. The 488 nm argon laser line was employed as excitation wavelength in the three samples.

299 to 295 and then to 292 nm for Pr 10, Pr 15 and Pr 20, respectively, suggest a decrease in the crystal field affecting the Pr^{3+} ion due to the increase in Pr–O distance leading to lower crystal fields. This is in agreement with the uniform

expansion that suffers the cubic F zirconia when its content of Pr^{3+} increases from 2.87 to 5.33 at.%, see Fig. 3.

Fig. 4 shows the absorption peaks in the region of 440–610 nm which were associated with electronic transitions within the 4f shell of Pr^{3+} ion, as follow: 447.9 nm: $^3H_4$–$^3P_2$; 471.5 nm: $^3H_4$–$^3P_1 + {}^1I_6$; 485.9 nm: $^3H_4$–$^3P_0$; 583 nm: $^3H_4$–$^1D_2$; and 609 nm: $^3H_4$–$^1D_2$. No changes in the position of these absorption peaks with the increase of Pr^{3+} concentration in zirconia (see zoom 2 of Fig. 4), and the subsequent decrease on crystal field, were observed. This is in agreement with the well shielded 4f electrons by the $5s^2$ and $5p^6$ electrons.

A red color emission resulted from the photoexcitation of praseodymium doped zirconia powders. A decrease in photoluminescence emission intensity with the increase of the doping concentration was observed at naked eye. Fig. 5 shows the photoluminescence results for mixed (Pr 1 sample), tetragonal (Pr 5 sample) and cubic (Pr 15) crystalline phases of praseodymium doped zirconia powders under photo excitation centered at 488 nm, which produces a direct excitation from $^3H_4$ to $^3P_{js}$ energy levels. The spectra show multiple peaks that were associated with the 4f inter-level electronic transitions in Pr^{3+} ions. This suggests different paths for Pr^{3+} returning to the base energy state. The location of the peaks and its associated 4f electronic transition are shown in Tables 2–4. The $^1D_2$–$^3H_4$ electronic transitions in Pr^{3+} ions were the responsible of the red color emission from zirconia. Differences between emission spectra for mixed (Fig. 5 – Pr 1), tetragonal (Fig. 5 – Pr 5) and cubic (Fig. 5 – Pr 15) crystalline phases of praseodymium doped zirconia, were found. Three emission peaks centered at 535, 586.4 and 598.4 nm, and associated with $^3P_1 + {}^1I_6 - {}^3H_5$ electronic transitions, were only present in tetragonal zirconia spectrum (Fig. 5 – Pr 5). Two emission peaks located at 653.2 and 655.4 nm, associated to $^3P_0$–$^3H_6$ electronic transitions, were only present in cubic zirconia spectrum (Fig. 5 – Pr 15). Remarkable changes on relative emission intensity between peaks corresponding to $^1D_2$–$^3H_4$ electronic transitions were observed for cubic zirconia as compared with relative intensity in mixed or

Table 2
Association of the peaks observed in the photoluminescent emission spectrum of monoclinic/tetragonal/cubic zirconia (Pr 1 sample), with 4f inter-level electronic transitions in Pr^{3+} ion

Wavelength (nm)	Transition	Wavelength (nm)	Transition	Wavelength (nm)	Transition
552.2	$^3P_1 + {}^1I_6 - {}^3H_5$ L	621.8	$^1D_2 - {}^3H_4$ sh	755.4	$^3P_0 - {}^3F_{3,4}$ vl
563.6	$^3P_1 + {}^1I_6 - {}^3H_5$ S	625.8	$^1D_2 - {}^3H_4$ m	761.4	$^3P_0 - {}^3F_{3,4}$ l
565.2	$^3P_1 + {}^1I_6 - {}^3H_5$ S	644.4	$^3P_0 - {}^3H_6$ s	835.2	$^1D_2 - {}^3F_2$ l
614.6	$^1D_2 - {}^3H_4$ s	670.6	$^3P_0 - {}^3H_6$ l	841.4	$^1D_2 - {}^3F_2$ l
615.8	$^1D_2 - {}^3H_4$ s	721.2	$^1D_2 - {}^3H_5$ m		
617.6	$^1D_2 - {}^3H_4$ m	743.4	$^3P_0 - {}^3F_{3,4}$ l		

s – strong intensity, m – medium intensity, l – low intensity, vl – very low intensity, and sh – shoulder.

Table 3
Association of the peaks observed in the photoluminescent emission spectrum of tetragonal zirconia (Pr 5 sample), with 4f inter-level electronic transitions in Pr^{3+}ion

Wavelength (nm)	Transition	Wavelength (nm)	Transition	Wavelength (nm)	Transition
535 *	$^3P_1 + {}^1I_6 - {}^3H_5$ m	615.2	$^1D_2 - {}^3H_4$ s	720.8	$^1D_2 - {}^3H_5$ m
552	$^3P_1 + {}^1I_6 - {}^3H_5$ L	617.6	$^1D_2 - {}^3H_4$ sh m	742.6	$^3P_0 - {}^3F_{3,4}$ l
563.6	$^3P_1 + {}^1I_6 - {}^3H_5$ sh	622	$^1D_2 - {}^3H_4$ sh	753.4	$^3P_0 - {}^3F_{3,4}$ l
565.2	$^3P_1 + {}^1I_6 - {}^3H_5$ S	625.8	$^1D_2 - {}^3H_4$ m	760.2	$^3P_0 - {}^3F_{3,4}$ l
586.4 *	$^3P_1 + {}^1I_6 - {}^3H_5$ l	643.4	$^3P_0 - {}^3H_6$ s	766.8	$^3P_0 - {}^3F_{3,4}$ vl
598.4 *	$^3P_1 + {}^1P_6 - {}^3H_5$ m	670.4	$^3P_0 - {}^3H_6$ m	834.4	$^1D_2 - {}^3F_2$ s
614.2	$^1D_2 - {}^3H_4$ s	711.4 *	$^1D_2 - {}^3H_5$ vl	841.2	$^1D_2 - {}^3F_2$ m

s – strong intensity, m – medium intensity, l – low intensity, vl – very low intensity, and sh – shoulder.

Table 4
Association of the peaks observed in the photoluminescent emission spectrum of cubic zirconia (Pr 15 sample), with 4f inter-level electronic transitions in Pr^{3+}ion

Wavelength (nm)	Transition	Wavelength (nm)	Transition	Wavelength (nm)	Transition
537.8	$^3P_1 + {}^1I_6 - {}^3H_5$ L	624.8	$^1D_2 - {}^3H_4$ s	668.6	$^3P_0 - {}^3H_6$ s
552.4	$^3P_1 + {}^1I_6 - {}^3H_5$ L	626.6	$^1D_2 - {}^3H_4$ sh	719.0	$^1D_2 - {}^3H_5$ m
565.4	$^3P_1 + {}^1I_6 - {}^3H_5$ l	642.4	$^3P_0 - {}^3H_6$ s	755.8	$^3P_0 - {}^3F_{3,4}$ l
615.4	$^1D_2 - {}^3H_4$ s	653.2	$^3P_0 - {}^3H_6$ m		
617.2	$^1D_2 - {}^3H_4$ s	655.4	$^3P_0 - {}^3H_6$ m		

s – strong intensity, m – medium intensity, l – low intensity, vl – very low intensity, and sh – shoulder.

tetragonal zirconia. The relative intensity of the 565.4 nm emission peak ($^3P_1 + {}^1I_6 - {}^3H_5$ electronic transition) for cubic zirconia, presented a considerable increase over the peaks associated to $^1D_2$–$^3H_4$ electronic transition, as compared with the results obtained for mixed phases and tetragonal zirconia. This indicates a considerable change on preferences in Pr^{3+} relaxation paths. Absence of 835.2 and 841.4 nm peaks in cubic zirconia spectrum ($^1D_2$–$^3F_2$ electronic transition), and its presence in mixed and tetragonal zirconia, was observed. In the emission spectrum for cubic zirconia a wide band is observed, on this band are mounted the typical Pr^{3+} emission peaks; that band was attributed to the intrinsic emission of zirconia [27]. Changes in relative intensity of the peaks and the absence and addition of new peaks in the emission spectrum for praseodymium doped zirconia, indicate new preferential paths for Pr^{3+} ion returning to the base energy state that were attributed to crystal field changes associated with the type of Pr^{3+} environment, which depends on crystalline structure of zirconia where they were incorporated. The above-mentioned is in agreement with the shift that suffers the $4f^3$–$4f^25d$ absorption band and the non changes in the position of the absorption peaks that were associated with 4f inter-level transitions in Pr^{3+} ion (see Fig. 4). The presence of intrinsic emission of zirconia and the lost in intensity of emission peaks associated with 4f inter-level electronic transitions in Pr^{3+} ions in cubic zirconia, were related with a decrease on the probability of Pr^{3+}–O^{2-} charge transfer by the increase of distance between praseodymium and oxygen ions due to the expansion of zirconia cubic cell.

3.3. Conclusions

Polycrystalline praseodymium doped zirconia powders with homogeneous chemical contents and crystallite size lower than 27 nm were obtained. Evidence of a homogeneous nucleation mechanism was observed. Zirconia powders with well defined tetragonal I and cubic F crystal structures were obtained under a relative low cost technique. Lattice parameters for tetragonal I zirconia were $a_T = 3.60$ Å, $c_T = 5.17$ Å. The increasing of Pr^{3+} ions in zirconia produces an expansion of zirconia cubic cell, resulting in lattice parameters of: 5.16, 5.18, and 5.20 Å for 2.87, 4.76 and 5.33 at.% contents, respectively. The incorporation of Pr^{3+} ion in zirconia induces deep energy levels in its energy gap due to the creation of crystal defects, which results in a wide absorption band centered at 380 nm. A preferred incorporation of Pr^{3+} in cubic C_2 sites was observed. A decrease on crystal field acting over Pr^{3+} ion with the increase of Pr^{3+} concentration was observed. The zirconia powders presented a red color emission associated with electronic transitions from the $^1D_2$ to the $^3H_4$ energy levels in Pr^{3+} ion. Photoluminescence emission spectra show multiple peaks and all were associated with electronic transitions within the 4f shell of Pr^{3+} ion. Significant differences in emission spectra for tetragonal and cubic zirconia were observed. Due to crystal field changes affecting Pr^{3+} ion, remarkable changes on preference of Pr^{3+} for certain returning paths to its base energy state were induced, which produces considerable changes in the emission color coming from praseodymium doped zirconia. Based on the fact that the thermo-luminescence response and sensitivity of ZrO_2 depend on the crystalline structure, this particular material could be used as a dosimeter for ionizing radiation, gamma, beta, X-ray and UV light.

Acknowledgments

The authors thank to José Guzmán, Leticia Baños, Lorena Uriarte and Francisco Ayala for technical support provided and CECyT (Sinaloa-México) and CONaCyT CB-2006-1-J1-I0002-57809 (México) for the financial grant for this investigation.

References

[1] M. García-Hipólito, A. Corona-Ocampo, O. Alvarez-Fregoso, E. Martínez, J. Guzmán-Mendoza, C. Falcony, Phys. Status Solidi (a) 201 (2004) 72.
[2] M. García-Hipólito, J. Guzmán-Mendoza, E. Martínez, O. Alvarez-Fregoso, C. Falcony, Phys. Status Solidi (a) 201 (7) (2004) 1510.
[3] M. García-Hipólito, O. Alvarez-Fregoso, J. Guzmán, E. Martínez, C. Falcony, Phys. Status Solidi (a) 201 (15) (2004) R127.
[4] R. Martinez-Martinez, M. Garcia-Hipólito, F. Ramos-Brito, J. L Hernández-Pozos, U. Caldiño, C. Falcony, J. Phys.: Condens. Mat. 17 (2005) 3647.
[5] G. Blasse, B.C. Grabmaier, Luminescent Materials, Springer, Berlin, 1994 (pp. 27–28, 40–50).
[6] E.C. Subbarao, Zirconia-an overview Science and Technology of Zirconia, in: A.H. Heuer, L.W. Hobbs (Eds.), Advances in Ceramics, vol. 3, The American Ceramic Society Inc, Columbus, OH, 1981, p. 1.
[7] P. Li, I.-W. Chen, J.E. Pender-Hahn, J. Am. Ceram. Soc. 77 (5) (1994) 1281.
[8] P. Li, I.-W. Chen, J. Am. Ceram. Soc. 77 (5) (1994) 1289.
[9] C.K. Loong, G.K. Liu, M. Ozawa, S. Suzuki, J. Alloys Compd. 300–3001 (2000) 147.
[10] M. Cole, C.R.A. Catlow, J.P. Dragun, J. Phys. Chem. Sol. 51 (1990) 507.
[11] M. Kunz, H. Kretschmann, W. Assmus, C. Klingshirn, J. Lumin. 37 (1987) 123.
[12] R.I. Merino, J.A. Pardo, J.I. Peña, G.F. De La fuente, A. Larrea, V.M. Orera, Phys. Rev. B 56 (1997) 10907.
[13] B. Savoini, J.E.M. Santiuste, R. Gonzalez, Phys. Rev. B 56 (1997) 5856.
[14] R.I. Merino, V.M. Orera, R. Cases, M.A. Chamarro, J. Phys. Condens. Mat. 3 (1991) 8491.
[15] F.S. De Vicente, A.C. Hernandes, M.F. De Souza, M.R.B. Andreeta, M. Siu Li, Rad. Effec. Def. Sol. 147 (1998) 77.
[16] F.S. De Vicente, A.C. Hernandes, A.C. De Castro, M.F. De Souza, M.R.B. Andreeta, M. Siu Li, Rad. Effec. Def. Sol. 149 (1999) 153.
[17] E. Pereyra Perea, M.R. Estrada-Yañez, M. García, J. Phys. D Appl. Phys. 31 (1998) L7.
[18] C. Urlacher, C. Marco de Lucas, E. Bernestein, B. Jacquier, J. Mugnier, Opt. Mater. 12 (1999) 19.
[19] R. Reisfeld, M. Zelner, A. Patra, J. Alloys Compd. 300–3001 (2000) 147.
[20] C. Laberty-Robert, F. Ansart, S. Castillo, G. Richar, Solid State Sci. 4 (8) (2002) 1053.

[21] F. Ramos-Brito, H. Murrieta S, J. Hernández A, E. Camarillo, M. García-Hipólito, R. Martínez-Martínez, O. Álvarez-Fragoso, C. Falcony, J. Phys. D: Appl. Phys. 39 (2006) 2079.
[22] B.D. Cullity, S.R. Stock, Elements of X-Ray Diffraction, Third ed., Prentice Hall, New Jersey, 2001, 302.
[23] P. Li, I-W. Chen, J.E. Pender-Hahn, Phys. Rev. B 48 (14) (1993) 10065.
[24] Dexpert Ghys, M. Faucher, P. Caro, J. Sol. State Chem. 54 (1984) 174.
[25] R.C. Garvie, J. Phys. Chem. 69 (4) (1965) 1238.
[26] G.C. Aumüler, W. Köstler, B.C. Grabmaier, R. Frey, J. Phys. Chem. Solid. 55 (8) (1994) 767.
[27] F. Ramos-Brito, M. García-Hipólito, R. Martínez-Martínez, E. Martínez-Sánchez, C. Falcony, J. Phys. D: Appl. Phys. 37 (2004) L13.